Multi-parameter least-squares reverse time migration using the viscoacoustic-wave equation

[1,2]Nogueira P. and [1]Porsani, M. ([1]UFBA/INCT-GP, [2]SENAI CIMATEC)

This paper was prepared for presentation during the 18^{th} International Congress of the Brazilian Geophysical Society held in Rio de Janeiro, Brazil, 16-19 October 2023.

Abstract

In viscoacoustic least-squares reverse time migration (QLSRTM) methods, the Q factor is assumed to be known, inverting only the velocity (v) parameter or v associated variables such as squared slowness or bulk modulus. However, the Q factor influences the amplitude and phase of the seismic data, especially in basins containing gas reservoirs or storing CO2. Therefore, the Q factor or Q associated parameters must be considered a model parameter to be inverted in the QLSRTM context. Thus, we propose a multi-parameter viscoacoustic least-squares reverse time migration (M-QLSRTM) procedure, which obtains the inverse of bulk modulus (κ) and the Q magnitude (τ) simultaneously. We derive and implement the multi-parameter forward and adjoint pair Born operators and the gradient formulas concerning κ and τ parameters. Then, we apply these operators and gradients in least-squares reverse time migration and, using our M-QLSRTM approach, estimate κ, and τ reflectivity models parameters with higher resolution when compared to conventional migration images.

Introduction

Saturated fluid reservoirs cause strong P-wave attenuation, which can degrade the resolution of seismic images. This is because the earth is anelastic and therefore decreases the amplitudes and distorts the phases of the seismic waves (Aki & Richards, 1980). In cases where the attenuation of the medium is too strong, neglecting it in the migration procedure can result in blurred amplitudes reflectors below the attenuating layers. P-wave attenuation can be measured through a quality factor Q, which accounts for the seismic wave's energy dissipation and phase distortion. Low Q-values imply more significant dissipated wave energy per cycle, mainly when the seismic pulse founds rocks as gas-sandstones and shales with very low-quality factors ($Q \approx 15-20$).

The first studies to restore the energy dissipated and repair waveform distortion were performed in the data domain using the Q filtering approach (Bickel & Natarajan, 1985; Hargreaves & Calvert, 1991). However, these data domain approaches fail to effectively correct the attenuation effects because the dissipation and dispersion phenomena occur during the wave propagation. Therefore approaches based on wave propagation are the most adequate and effective to compensate for the Q effects.

Mu et al. (2021) developed a viscoacoustic wave equation in the time domain to simulate wave propagation in anelastic media. They proposed a new viscoacoustic wave equation inserting the complex-valued phase velocity derived from the Kjartansson attenuation model in the frequency-wavenumber domain in the acoustic wave equation. The proposed equation has one second-order temporal derivative and two spatial variable-order fractional Laplacian operators describing the pulse distortion and amplitude dissipation effects. The results indicate that their viscoacoustic equation is more accurate than the traditional fractional viscoacoustic wave equation that describes constant-Q attenuation.

In the viscoacoustic least-squares reverse time migration (QLSRTM), the pioneering work is from Dutta & Schuster (2014). Thus, to correct the waveform distortion, Dutta & Schuster (2014) implemented, based on the SLS mechanical model, a linearized Born viscoacoustic modeling operator. They also implemented the backward propagation based on the adjoint method using an elegant matrix formalism and consequently obtained the gradient formula concerning the bulk modulus parameter. Using that, they built a QLSRTM inversion scheme, showing that considering the attenuation phenomena in their inversion procedures, they produced images with better-balanced amplitudes and higher resolution below the attenuating layers. Yang & Zhu (2019) propose a complex-valued QLSRTM. They insert the complex-valued velocity in the acoustic wave equation. Using a second-order polynomial to approximate the dispersion term and a pseudo-differential operator to rewrite the dissipation term, they derive a complex-valued viscoacoustic equation. Based on this equation, they derive the forward and adjoint operators and implement the QLSRTM algorithm with total variation regularization to optimize the scheme and use the Hessian diagonal as a preconditioner to accelerate method convergence.

The previously mentioned works performed a single-parameter QLSRTM approach, considering that only a single parameter is responsible for the reflectivity model. Usually, the considered parameter is the v model or v associated models, such as bulk modulus and squared slowness. However, depending on the subsurface surveyed, the seismic data can contain strong viscous, elastic, and anisotropic effects. Thus, a multi-parameter QLSRTM approach that considers both v and Q associated perturbation as reflectivity models $\delta\mathbf{m}$ (i.e., the seismic images) is crucial in the inversion scheme, mainly when

the physical medium is very attenuating. Thus, we propose a multi-parameter QLSRTM (M-QLSRTM) seismic inversion approach, where we perturb the inverse of the bulk modulus and the Q magnitude, both directly related to the velocity and Q factor, respectively. We highlight the importance of considering the Q factor in the seismic inversion procedure, especially in a strongly attenuating.

Non-linear viscoacoustic modeling operator

In a viscoacoustic media, the calculated wavefield can be obtained from the relationship between the pressure wavefield and the particle velocity considering a single SLS (Robertsson et al., 1994):

$$\frac{\partial p}{\partial t}+\left[K\left(1+\tau e^{-\frac{t}{\tau_\sigma}}\right)\delta(t)-K\frac{\tau}{\tau_\sigma}\left(e^{-\frac{t}{\tau_\sigma}}H(t)\right)\right]*\nabla\cdot\mathbf{v}=0, \tag{1}$$

and

$$\frac{\partial \mathbf{v}}{\partial t}+b\nabla p=0, \tag{2}$$

where $\tau=\tau_\varepsilon/\tau_\sigma-1$ represents the magnitude of Q. τ_ε and τ_σ are, respectively, the relaxation time *stress* and *strain*, given by:

$$\tau_\sigma=\frac{\sqrt{Q^2+1}-1}{2\pi f_0 Q} \quad \text{and} \quad \tau_\varepsilon=\frac{\sqrt{Q^2+1}+1}{2\pi f_0 Q}, \tag{3}$$

being $K=K(\mathbf{x})$ is the bulk modulus at the position $\mathbf{x}$, $b=b(\mathbf{x})$ is the buoyancy, p is the pressure wavefield, $\mathbf{v}=\mathbf{v}(\mathbf{x},t)$ is the particle velocity vector, and $H(t)$ is the Heaviside function. The symbol * represents a time convolution in the equation ((1)).

Taking the time derivative in (1)

$$\frac{\partial^2 p}{\partial t^2}+\left[K\left(1+\tau e^{-\frac{t}{\tau_\sigma}}\right)\delta(t)-K\frac{\tau}{\tau_\sigma}\left(e^{-\frac{t}{\tau_\sigma}}H(t)\right)\right]*\nabla\cdot\frac{\partial \mathbf{v}}{\partial t}=0, \tag{4}$$

substituting (2) in (4)

$$\kappa\frac{\partial^2 p}{\partial t^2}-\nabla\cdot b\nabla p-\tau\nabla\cdot b\nabla p+\frac{\tau}{\tau_\sigma}e^{-\frac{t}{\tau_\sigma}}H(t)*\nabla\cdot b\nabla p=0, \tag{5}$$

where κ is the inverse of the bulk modulus, the equation system (5) describes the non-linear viscoacoustic forward equation. However, equation (5) is computationally expensive to solve numerically due to the convolution term existence. Robertsson et al. (1994) simplifies the convolution term by introducing a memory variable, resulting in a computationally solvable equation system. Thus, the non-linear forward modeling becomes

$$\begin{cases}\kappa\dfrac{\partial^2 p}{\partial t^2}-\nabla\cdot b\nabla p-\tau\nabla\cdot b\nabla p+r_p=f,\\ \dfrac{\partial r_p}{\partial t}=\dfrac{\tau}{\tau_\sigma}\nabla\cdot b\nabla p-\dfrac{1}{\tau_\sigma}r_p,\end{cases} \tag{6}$$

where r_p is a memory variable responsible for the wavefield attenuation. The equation system (6) describes the non-linear forward modeling for a viscoacoustic medium Carcione et al., 1988; Blanch et al., 1995; Bai et al., 2014.

We use the vector $\mathbf{w}=[p \quad r_p]^T$ to denote wavefield. The seismic data are sampled at receiver positions as $\mathbf{d}=\mathbf{R}\mathbf{w}$ with $\mathbf{d}=[d \quad 0]^T$. In this work, we use equation (5) to derive the multi-parameter Born modeling equation.

Multi-parameter linearized viscoacoustic modeling operator

According to the perturbation theory, the physical parameters can be expressed as the sum of the background and perturbed parameters (Dutta & Schuster, 2014):

$$\begin{cases}b=b_0+\delta b,\\ \kappa=\kappa_0+\delta\kappa,\\ \tau_\sigma=\tau_{\sigma_0}+\delta\tau_\sigma,\\ \tau=\tau_0+\delta\tau.\end{cases} \tag{7}$$

where b_0, K_0, τ_{σ_0}, and τ_0 are background medium parameters and δb, δK, $\delta\tau_\sigma$ and $\delta\tau$ denotes the parameter perturbations. Here, we assume that the medium parameters b and τ_σ are accurate, that is, $\delta b=0$ and $\delta\tau_\sigma=0$. Unlike the single-parameter inversion approaches (Dutta & Schuster, 2014; Witte et al., 2019; Mu et al., 2020), we implement a multi-parameter inversion approach. We consider that the subsurface reflectivity model represents the perturbations of the inverse of bulk modulus ($\delta\kappa$) and magnitude of quality factor ($\delta\tau$). Consequently, a perturbation in these parameters causes a wavefield perturbation. Thus, the pressure wavefield $p(\mathbf{x},t)$ can be linearized as

$$p(\mathbf{x},t)=p_0(\mathbf{x},t)+\delta p(\mathbf{x},t), \tag{8}$$

where $p_0(\mathbf{x},t)$ and $\delta p(\mathbf{x},t)$ are the background and perturbed wavefields, respectively. Then, the perturbed wavefield δp can be written as

$$\begin{cases}\kappa_0\dfrac{\partial^2\delta p}{\partial t^2}-\nabla\cdot b_0\nabla\delta p-\tau_0\nabla\cdot b_0\nabla\delta p+\delta r=-\delta\kappa\dfrac{\partial^2 p_0}{\partial t^2}+\\ \delta\tau\nabla\cdot b_0\nabla p_0-\delta\tau\dfrac{r_0}{\tau_0},\\ \dfrac{\partial\delta r}{\partial t}=\dfrac{\tau_0}{\tau_{\sigma_0}}\nabla\cdot b_0\nabla\delta p-\dfrac{\delta r}{\tau_{\sigma_0}}.\end{cases} \tag{9}$$

The multi-parameter linearized viscoacoustic modeling operator can be expressed in abstract form as

$$\delta\mathbf{d}=\mathbf{L}\delta\mathbf{m} \tag{10}$$

where $\delta\mathbf{d}$ is data perturbation, $\delta\mathbf{m}=[\delta\kappa \quad \delta\tau]^T$ denotes model perturbation and operator $\mathbf{L}$ indicates the viscoacoustic Born approximation operator.

Multi-parameter linearized adjoint operator and gradient formulas in viscoacoustic media

The migration operator is the adjoint of the Born modeling operator that maps the seismic reflection data $\delta\mathbf{d}$ to the perturbation model $\delta\mathbf{m}$. Thus, considering the background medium parameters, the adjoint equations for equation (6) can be obtained through the adjoint-state method and is

given by (Blanch & Symes, 1995; Dutta & Schuster, 2014) and is given by

$$\begin{cases} \kappa_0 \dfrac{\partial^2 q}{\partial t^2} - \nabla \cdot b_0 \nabla (1+\tau_0) q - \nabla \cdot b_0 \nabla \dfrac{\tau_0}{\tau_{\sigma_0}} r_q = \Delta d, \\ \dfrac{\partial r_q}{\partial t} - \dfrac{r_q}{\tau_{\sigma_0}} - q = 0. \end{cases} \tag{11}$$

where q and r_q are the adjoint-state variable of the state variables p and r_p, respectively. Δd is the pressure data residual between the calculated and the observed data.

The perturbation model $\delta \mathbf{m} = [\delta\kappa \quad \delta\tau]^T$, which corresponds to the gradient of the M-QLSRTM, is given by

$$\delta\kappa = \frac{\partial J}{\partial \kappa_0} = -\int_0^T \frac{\partial^2 p_0}{\partial t^2} q \;\; dt \tag{12}$$

and

$$\delta\tau = \frac{\partial J}{\partial \tau_0} = \int_0^T (\nabla \cdot b_0 \nabla p_0) q + (\frac{1}{\tau_{\sigma_0}} \nabla \cdot b_0 \nabla p_0) r_q \;\; dt \tag{13}$$

Theory of M-QLSRTM

Based on linear inversion theory, M-QLSRTM aims to estimate the optimal subsurface reflectivity image (Dutta & Schuster, 2014). Thus, the misfit function can be written as

$$J(\mathbf{m}) = \frac{1}{2} ||\delta\mathbf{d} - \mathbf{d}^{obs}||_2^2 = \frac{1}{2} ||\mathbf{L}\delta\mathbf{m} - \mathbf{d}^{obs}||_2^2, \tag{14}$$

where $\delta\mathbf{d}$ and $\mathbf{d}^{obs}$ are the Born modeled data and the observed data, respectively. $\mathbf{L}$ is the Born modeling operator and $\delta\mathbf{m} = [\delta\kappa \;\; \delta\tau]^T$ is the reflectivity model. So, $\delta\mathbf{m}$ can be estimated by the conjugated-gradient method (CGM). The implementation for CGM is as follows:

$$\begin{aligned} \mathbf{g}^{k+1} &= \mathbf{L}^T [\mathbf{L}\delta\mathbf{m}^k - \mathbf{d}^{obs}], \\ \beta^{k+1} &= \frac{[\mathbf{g}^{k+1}]^T \mathbf{g}^{k+1}}{[\mathbf{g}^k]^T [\mathbf{g}^k]}, \\ \mathbf{z}^{k+1} &= \mathbf{g}^{k+1} + \beta^{k+1} \mathbf{z}^k, \\ \alpha^{k+1} &= \frac{[\mathbf{z}^{k+1}]^T [\mathbf{g}^{k+1}]}{[\mathbf{L}\mathbf{z}^{k+1}]^T [\mathbf{L}\mathbf{z}^{k+1}]}, \\ \delta\mathbf{m}^{k+1} &= \delta\mathbf{m}^k - \alpha^{k+1} \mathbf{z}^{k+1}, \end{aligned} \tag{15}$$

where k represents the iteration index, $\mathbf{g}^k$ and β^k are the gradient and the step-length, $\mathbf{z}^k$ and α^k are the conjugate gradient direction and the corresponding step-length, T represents the conjugate transpose of a matrix. According to M-QLSRTM with CGM shown, we use an M-QLSRTM, which includes five steps. The first step is to obtain the calculated data through multi-parameter Born modeling, then compute the residual data by subtracting the calculated data from observed data. Thus, we calculate the objective function using data residual as the adjoint source for backpropagation. The third step calculates the conjugate gradient direction and the corresponding step length using the gradient computed in the second step. The fourth step updates the current reflectivity model using the previously computed conjugate gradient direction. This procedure occurs until reaching a pre-established number of iterations.

Numerical experiments

We demonstrate the feasibility of M-QLSRTM with synthetic data. Numerical examples are for Overthrust model. We generate the observed data in numerical examples with equation (9). We note that initial reflectivity images concerning κ and τ parameters refer to the first iteration of M-QLSRTM. We test the sensitivity of the proposed M-QLSRTM considering different errors in the τ model. Finally, to show the robustness of the proposed M-QLSRTM, we also test the M-QLSRTM for different noise levels in observed data.

Overthrust model

The M-QLSRTM approach is now tested on the land overthrust model. Figure 1 a and b show the true velocity and Q models used to calculate the $\delta\kappa$ (Figure 1 c) and $\delta\tau$ (Figure 1 d) models reflectivity, and from it to generate the observed data in which contains 400 shots excited with a $50\ m$ shot interval at a depth of $30\ m$. Each shot is recorded with 800 receivers and a $25\ m$ receiver interval with a recording time of $4\ s$.

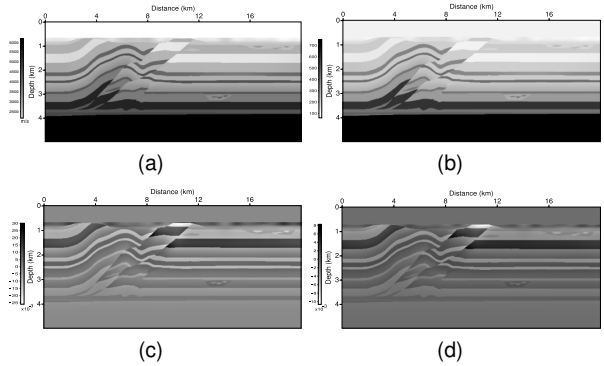

Figure 1 – Overthrust model: True velocity model (a), True Q model (b), True $\delta\kappa$ reflectivity model (c) and True $\delta\tau$ reflectivity model (d).

Using the true reflectivities models (Figure 1c) and $\delta\tau$ (Figure 1d), we generated the observed data and applied the M-QLSRTM. First, we obtain the initials $\delta\kappa$ and $\delta\tau$ (Figures 2a and c) reflectivities images, which correspond to the first iteration of M-QLSRTM procedure. So, at the end of 20 iterations, we get the final reflectivities images concerning the $\delta\kappa$ (Figure 2b) and $\delta\tau$ (Figure 2d). These final images contain higher resolution when compared to initial images (Figures 1a and c). The M-QLSRTM inversion scheme highly reduced the low-frequency noise and improved the delineation of reflectors for both $\delta\kappa$ and $\delta\tau$ parameters. Figure 4a shows the decrease of the objective function for each iteration.

We compared vertical profiles for M-QLSRTM results. In Figure 3, we can analyze, on the left and the right, a comparison between the profiles for the reflectivities $\delta\kappa$ and $\delta\tau$, respectively. On both sides, the green curve is closer to the red curve than the blue curve. This result means that the inverted reflectivity models were successful in the M-QLSRTM scheme, evidencing the effectiveness of the implemented inverse procedure.

The convergence curve to M-QLSRTM is plotted in Figure 4, showing that the convergence of M-QLSRTM occurs.

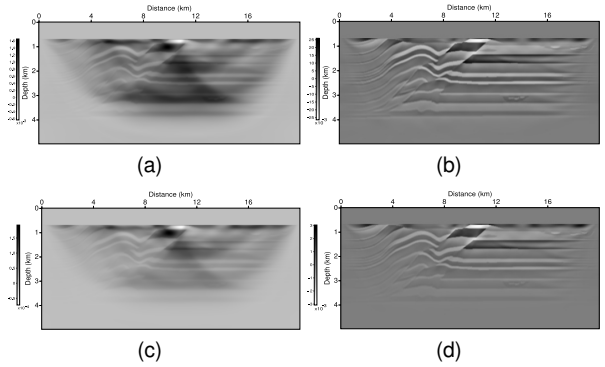

Figure 2 – Overthrust: Reflectivity model for initial $\delta\kappa$ (a), M-QLSRTM $\delta\kappa$ after 20 iterations (b), Initial $\delta\tau$ (c), M-QLSRTM $\delta\tau$ after 20 iterations (d).

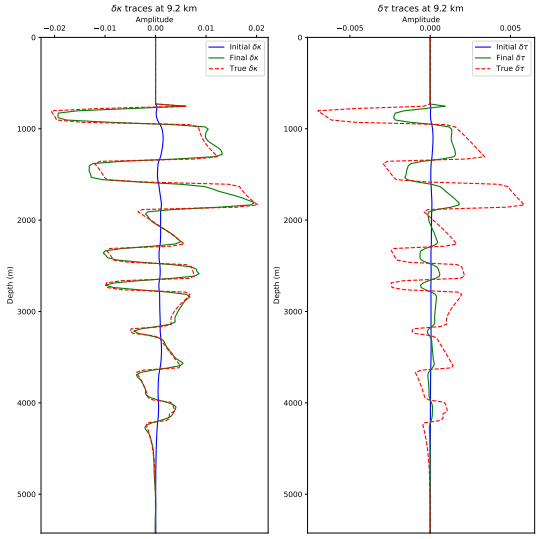

Figure 3 – Vertical profiles at central position for Overthrust experiment. Comparison for $\delta\kappa$ reflectivity (left), and comparison for $\delta\tau$ reflectivity (right).

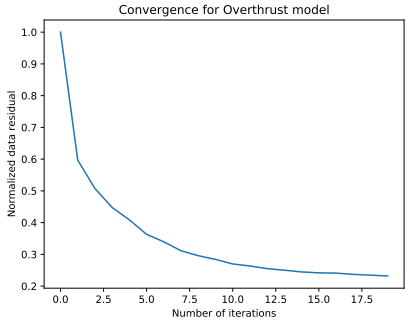

Figure 4 – Convergence curve for M-QLSRTM for Overthrust experiment.

Sensitivity of M-QLSRTM to random seismic noise

We now test the sensitivity of the proposed M-LSRTM to random noise. The random noise was applied from the signal-to-noise ratio, expressed in decibels (dB), with the following equation:

$$S/N = 10\log_{10}\Big(As/An\Big), \tag{16}$$

where $As = ||\vec{d}_s||^2$ is the signal energy and $An = ||\vec{d}_s - \vec{d}_{s+n}||^2$ is the noise energy (Wilson et al., 1997). $\vec{d}_s$ is the signal of the observed data, $\vec{d}_{s+n}$ is the signal of the noisy observed data.

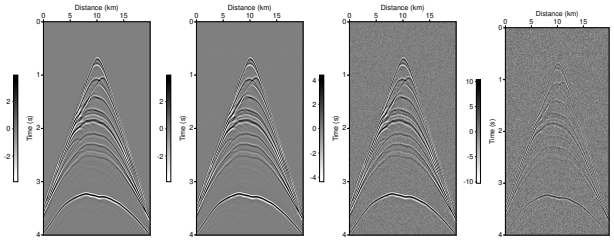

Figure 5 – Central shot of the Overthrust data with different S/Ns.

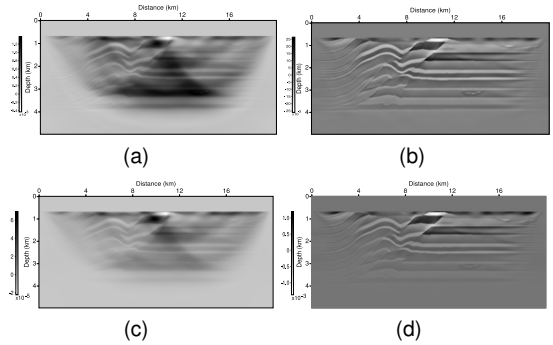

Figure 6 – M-QLSRTM for Overthrust data with S/N=30 dB. Reflectivity model for initial $\delta\kappa$ (a), final $\delta\kappa$ (b), initial $\delta\tau$ (c) and final $\delta\tau$ (d).

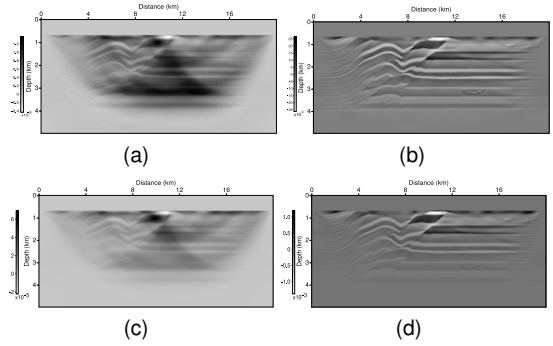

Figure 7 – M-QLSRTM for Overthrust data with S/N=14 dB. Reflectivity model for initial $\delta\kappa$ (a), final $\delta\kappa$ (b), initial $\delta\tau$ (c) and final $\delta\tau$ (d).

Figure 5 show the central shot of Overthrust data, with different signal-to-noise ratios (S/Ns). From these noisy data, we run M-QLSRTM. Figures 6, 7, 8 show the M-QLSRTM inverted models for the experiments using Overthrust data considering different noise levels. Figure 9 show for Overthrust data, the convergence curve considering the seismic data with different noise levels.

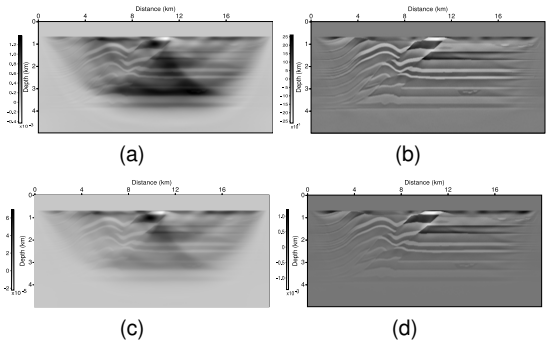

Figure 8 – M-QLSRTM for Overthrust data with S/N=3 dB. Reflectivity model for initial $\delta\kappa$ (a), final $\delta\kappa$ (b), initial $\delta\tau$ (c) and final $\delta\tau$ (d).

The experimental results show that a higher S/N of the data can obtain a better imaging result. The noise intensity in the imaging results increases with the decreasing S/N of the data. Analyzing Figure 9, we conclude that the M-QLSRTM is always robust and convergent under different S/N.

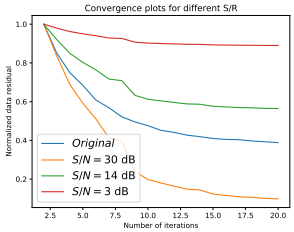

Figure 9 – Convergence curves for M-QLSRTM with different S/Ns for Overthrust data.

Conclusions

We present a time-domain M-QLSRTM method that uses the multi-parameter viscoacoustic wave equation to jointly estimate the inverse of bulk modulus and Q magnitude and consequently to compensate for the distortion in amplitudes and phases of seismic waves propagating in attenuative layers. Numerical results on synthetic data validate our proposed approach, showing that the multi-parameter linearized viscoacoustic wave equation and its adjoint equations used in the M-QLSRTM scheme can compensate for the loss attenuation during the iterations. In the results, our M-QLSRTM procedure produces $\delta\kappa$ and $\delta\tau$ reflectivities images with better-balanced amplitude and accurately positioned reflectors compared with its respective initials reflectivities images, even with the seismic data generated in the presence of noise, evidencing the robustness of the M-QLSRTM.

Acknowledgements

This study was financed by the project PIE00005/2016 of Infrastructure Edictal of FAPESB 003/2015 and was financed in part by the Coordenação de Aperfeiçoamento de Pessoal de Nível Superior-Brasil (CAPES)-Finance Code 001.

This work was executed in partnership between SENAI CIMATEC and PETROBRAS. The first author would like to acknowledge PETROLEO BRASILEIRO S.A and Agência Nacional de Petróleo, Gás Natural e Biocombustível (ANP), for the support and investments in R&D.

We wish to thank the Supercomputing Center for Industrial Innovation at SENAI CIMATEC for the support in this research, and INCT-GP/CNPq for financial support.

References

Aki, K. & Richards, P., 1980. Quantitative Seismology: Theory and Methods, Freeman.

Bai, J., Yingst, D., Bloor, R. & Leveille, J., 2014. Viscoacoustic waveform inversion of velocity structures in the time domain: Geophysics, 79, R103–R119.

Bickel, S. & Natarajan, R., 1985. Plane-wave q deconvolution, Geophysics, vol. 50(9): 1426–1439.

Blanch, J. O., Robertsson, J. O. & Symes, W. W., 1995. Modeling of a constant q: Methodology and algorithm for an efficient and optimally inexpensive viscoelastic technique, Geophysics, vol. 60(1): 176–184.

Blanch, J. O. & Symes, W. W., 1995. Efficient iterative viscoacoustic linearized inversion, in: SEG Technical Program Expanded Abstracts 1995, Society of Exploration Geophysicists.

Carcione, J. M., Kosloff, D. & Kosloff, R., 1988. Wave propagation simulation in a linear viscoelastic medium, Geophysical Journal International, vol. 95(3): 597–611.

Dutta, G. & Schuster, G. T., 2014. Attenuation compensation for least-squares reverse time migration using the viscoacoustic-wave equation, Geophysics, vol. 79(6): S251–S262.

Hargreaves, N. D. & Calvert, A. J., 1991. Inverse q filtering by fourier transform, Geophysics, vol. 56(4): 519–527.

Mu, X., Huang, J., Wen, L. & Zhuang, S., 2021. Modeling viscoacoustic wave propagation using a new spatial variable-order fractional laplacian wave equation, Geophysics, vol. 86(6): T487–T507.

Mu, X., Huang, J., Yang, J., Guo, X. & Guo, Y., 2020. Least-squares reverse time migration in tti media using a pure qp-wave equation, Geophysics, vol. 85(4): S199–S216.

Robertsson, J. O., Blanch, J. O. & Symes, W. W., 1994. Viscoelastic finite-difference modeling, Geophysics, vol. 59(9): 1444–1456.

Wilson, T. A., Rogers, S. K. & Kabrisky, M., 1997. Perceptual-based image fusion for hyperspectral data, IEEE Transactions on Geoscience and Remote Sensing, vol. 35(4): 1007–1017.

Witte, P. A., Louboutin, M., Luporini, F., Gorman, G. J. & Herrmann, F. J., 2019. Compressive least-squares migration with on-the-fly fourier transforms, Geophysics, vol. 84(5): R655–R672.

Yang, J. & Zhu, H., 2019. Viscoacoustic least-squares reverse time migration using a time-domain complex-valued wave equation, Geophysics, vol. 84(5): S479–S499.